

Automatic GPU-based algorithm for OMERACT-RAMRIS score quantification in rheumatoid arthritis

L. Cesario¹, P. Parascandolo¹, L. Vosilla¹, G. Troglia¹, and G. Viano^{1†}

¹Softeco Sismat Srl, Genoa, Italy

Abstract

Rheumatoid Arthritis (RA) is a systemic disease that affects the synovial joints. Currently, the gold standard measurement for tracking the progression of the disease involves a semi-quantitative assessment of bone erosion, bone marrow edema, and synovitis in Magnetic Resonance Images. The Outcome Measures in Rheumatology Clinical Trials (OMERACT) Rheumatoid Arthritis Magnetic Resonance Imaging Score (RAMRIS) system represents a useful standard for the assessment of RA. However, the use of RAMRIS system is time-consuming and tedious and requires a long learning curve. The work presented in this paper is aimed at identifying how computer automation, using parallel computing on the Graphics Processing Unit (GPU), can be used to quantify OMERACT-RAMRIS score. The proposed algorithm is fully integrated in a Computer Aided Diagnosis (CAD) system named RheumaS-CORE (Softeco Sismat Srl) and enables users—even non-expert ones—to evaluate bone erosion in a short time and with little training. Preliminary results of qualitative and quantitative validation are presented and discussed at the end of the paper.

1. Introduction

Rheumatoid Arthritis (RA) is a chronic inflammatory autoimmune disease that affects synovial joints and leads to the destruction of periarticular bones. Bone erosions are localized lesions with a break in the cortical shell. Since bone erosions are closely related to the disease activity, they constitute an early prognostic indicator and an important clinical parameter to monitor treatment effectiveness [TC11, SRS13, FGC07]. It is therefore desirable to detect them as early as possible with high precision, in order to quantify small changes.

Currently, the gold-standard measurement for tracking the progression of the disease involves a semi-quantitative assessment of bone erosion, bone marrow edema, and synovitis in Magnetic Resonance Imaging (MRI), performed by a musculoskeletal radiologist.

The work presented in this paper shows how computer automation can be used to measure bone erosion volumes in MRI images, using OMERACT-RAMRIS, without the

expert and time-consuming intervention of a radiologist. A novel automatic 3D approach for the identification and quantification of bone erosions (i.e., the missing parts of the bone), to be used in the clinical practice, is described and evaluated here.

With respect to the literature, the proposed algorithm is based not on the direct segmentation of the erosion, but on the segmentation of the bone of interest, the reconstruction of its original shape, and the comparison between the segmented shape and the original one. A Statistical Shape Model (SSM) is extracted from a collection of training samples of segmented healthy bones; the model comprises the mean shape and a number of modes of variation obtained through a Principal Component Analysis (PCA). The healthy bone shape can be obtained as a linear combination of the mean shape and the modes of variation: the reconstruction of the original bone shape is obtained by calculating the best coefficients of this linear combination. The difference between the segmented bone and the reconstructed bone is the erosion of which it is possible to calculate the volume and the scoring.

Thanks to the use of Graphics Processing Units (GPUs), such as those commonly found on consumer-level personal computers, the automatic erosion scoring for all wrist bones

[†] The authors wish to thank Esaote Spa and DIMI (Dipartimento di Medicina Interna, Clinica Reumatologica, Università degli Studi di Genova) for their collaboration

(or hand bones) takes less than one minute. This leads to a substantial reduction of diagnosis time and costs, achieving high quality results in a very short time. The proposed approach is implemented using the *OpenCL* platform, which represents an independent standard holding high potential for exploiting the massive parallelism of modern multi-core processors and graphics processors.

The effectiveness of the proposed method is assessed by presenting both qualitative and quantitative results of wrist/hand bones considering pathological RA cases. To this purpose, the algorithm is fully integrated in a CAD system named RheumaSCORE [Rhe, BPV*12, CRP*13, PCVV14].

The paper is organized as follows. Section 2 gives an overview of the existing techniques and tools for RA scoring. Then details on reconstruction shape, segmentation and volume evaluation algorithms and GPU computing are provided. Section 3 provides the description of the proposed algorithm and the evaluation of its performance. Section 4 describes the integration of the implemented algorithm in the RheumaSCORE software. Section 5 includes a preliminary quantitative analysis of the approach when used in the clinical setting. Finally, in Section 6 conclusions are drawn.

2. Background and previous work

2.1. Rheumatoid arthritis scoring

Conventional Radiographs (CRs) are used to semi-quantitatively assess bone erosions in patients with RA. However, due to their projectional character, the use of CRs results in an underestimation of the number and size of erosions and, therefore, the eventual disease activity. Furthermore, it has been reported that it takes 6-12 months before structural changes become evident on CRs [Sok08], impeding the early validation of treatment efficacy.

Other imaging modalities have emerged, which allow a more sensitive detection of early bone erosions. MRI (Magnetic resonance Imaging) has demonstrated to be more sensitive than radiography for the detection of erosive bone changes in RA, especially the subtle changes that occur in the early phase of rheumatic diseases [MSC*98, COM*03, LVHp*06]. The Outcome Measures in Rheumatology (OMERACT) Rheumatoid Arthritis MRI Scoring System (RAMRIS) has been developed [OPC*03, LMO*03] with data from iterative multicenter studies [OPC*03, OKL*01, CLO*03]. The OMERACT RAMRIS is a semi-quantitative scoring system for assessing synovitis, bone erosions, and bone edema on MRI in RA hands and wrists. Studies on the quantification of bone erosions using MRI have previously shown reliability and feasibility [BLSE03, BEM*03], and they can be beneficial in documenting progression or regression of structural joint damage.

Also multidetector Computed Tomography (CT) has an important role in monitoring damage progression in RA. Anyways, unlike MRI, CT does not depict inflammation.

Some methods for the semi-automated quantification of erosions have been proposed for CT and MRI datasets. Duryea et al. [DMA*08], using CT data, describe a semi-automatic outlining of the periosteal surface followed by an erosion segmentation based on region growing. The studies performed by Døhn et al. [DEH*08], using CT data, and by Bird et al. [BLSE03] and Crowley et al. [CDM*11], using MRI data, rely on manual outlining of the erosions, slice by slice. While a trained operator may produce reliable results, manual outlining can be very time consuming. Moreover, a slice-wise approach does not take the true 3D erosion structure into account.

In contrast, Emond et al. [EIC*12] employ a 3D segmentation of erosions in MRI. Only the placement of a seed point and the selection of five parameters are required. However, this approach brings the complexity related to the choice of the parameters to segment the erosion.

In addition, to the best of our knowledge, there is no commercial framework for wrist/hand erosion scoring designed for MRI data. In that sense, a first result is the algorithm proposed here, which has been fully integrated in the RheumaSCORE software [Rhe, BPV*12, CRP*13, PCVV14], a specific CAD system for RA.

2.2. Reconstruction from pathological shapes

In RA scoring, a central issue is how to reconstruct pathological anatomical structures, when the original normal situation is unknown. Statistical models of healthy shapes allow to reconstruct pathological shapes in an automatic and reproducible way. The idea is to fit the statistical model to match the pathological shape in healthy regions. The resulting best fit will provide a patient-specific yet objective proposal for the re-modeling process.

Statistical models are widely used to represent the shape and appearance of objects, which can vary [HM09]. The Statistical Shape Models (SSMs) were introduced by Cootes and Taylor [CTG95]. Given a training set of shapes (each one represented by a set of points, a mesh, or an image), a linear model is learnt which describes any new shape as the sum of a mean and a weighted combination of “modes of variation”. The weights, which are called shape parameters, give a compact encoding of any particular shape.

Describing the shape of an object is a nontrivial task, which is commonly performed by employing meshes or images. Meshes consist of points in specific locations and the connections among them. They can be contours that surround a 2D area [RCA03], surface meshes that cover a volume [WHD*11] or volumetric meshes that contain points within the volume [SRE*06]. For the images, two different approaches have been proposed: distance maps [AAF*10] and the intensity image within the object of interest [LKH*09]. Here we adopt the distance map to represent the bone healthy shape.

The hypothesis underpinning our approach is that the shape of bones affected by a pathology departs from statically normal bone shape variation. When a pathological bone sample is registered with a SSM built from healthy bones, any diseased region will be represented as a departure from the model. Such regions can then be characterized as erosions and have their morphology and volume assessed. SSMs describe the variation that exist within a set of aligned training shapes. They are commonly used to identify shape instances in medical image data by utilizing the variability extracted from the training set by Principal Component Analysis (PCA) [CTG95]. In building such a model, it is necessary to establish point correspondences across the training set. This is often achieved by registering a single reference into each sample, using algorithms such as iterative closest point (rigid) and B-spline free form deformation (non-rigid) [KLZH09].

2.3. Segmentation and volume evaluation

Volumetric measurements are essential to evaluate the success of a therapy. As an example, the reduction of bone erosion volume determines the success of the treatment. In general, the measurement process can be organized into two steps: first, we need to select the relevant structure (*volume selection with segmentation*), and second, we need to compute the respective volume of that structure (*volume measurement*).

Segmentation is an important task in medical imaging, in order to recognize anatomical or pathological structures and determine their relevant characteristics such as size, shape, and volume. Moreover, image segmentation is the prerequisite for many interaction techniques to explore data and to carry out treatment planning.

In the context of RA, there is relatively little work on segmentation of wrist bones in 3D MRI sequences. Sebastian et al. [STCK03] describe an approach to segment carpal bones from Computed Tomography (CT) sequences using skeletally coupled deformable models. Similarly, Duryea et al. [DMA*08] describe their semi-automated approach using CT data. Koch et al. [KSCPI1] and Wodarczyk et al. [WCT*15] developed wrist segmentation framework on 3D MRI images. Parascandolo et al. [PCV*13] implemented a novel tool, called Smart Brush, for real-time interactive 3D image segmentation. The tool exploits GPU implementation of the sparse field level-set method, using OpenCL. It enables simple and user friendly interaction and enables a full 3D segmentation of a whole anatomical element, requiring only minimal interaction on 2D slices.

Once all voxels of a target structure are identified, the structure volume can be approximated for volumetry. A straightforward approach is to weight every voxel belonging to that selection with the size of a respective volume cell (voxel counting algorithm). This method achieves a reasonable approximation for interior core voxels. However, it does

not reflect the boundary voxels properly, where the separating isosurface may be closer or farther away from the voxels depending on the voxel values and the threshold. While this difference is almost negligible for compact selections—which have a relatively small boundary—it can be significant for small or elongated structures, like erosions.

Modified voxel counting [KFC89] estimates the volume as the sum of voxels inside the object plus half the sum of voxels on the surface. A better approach (voxel counting with edge resampling) is described in [BOG04] and adopted in this work. First, the boundary voxels are examined in their volume cell context, where a boundary cell contains between one and seven selected voxels (see Figure 1). Similar to the case table of the Marching Cubes approach [LC87], the boundary cells are classified into simple (one or seven voxels are selected) and complex cases (from two to six voxels are selected). Simple cases can be immediately resolved by weighting the respective volume with the interpolated isovalue parameter. The complex cases are recursively divided into eight subcells using trilinear interpolation until either only simple cases remain or the respective full voxel volume is below an error threshold.

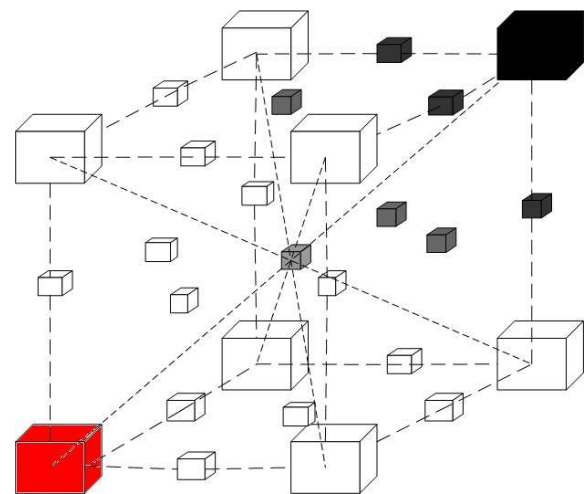


Figure 1: Voxel counting with edge resampling. The voxel in red (*R*) is interpolated as adjacent to the black one (belonging to the edge of the segmented element). The subdivision is done according to the voxel neighbors. The small cubes indicate the levels to be assigned to the $3 \times 3 \times 3$ subvoxel interpolation in which *R* will be divided. At this point, the contribution of “non-empty” subvoxels of *R* is added to the total volume.

2.4. GPU Computing

To overcome the computationally demanding tasks of medical image applications, researchers are moving to parallel computing on GPU. Recent GPUs demonstrate enormous

potential for scientific computing tasks in the form of General Purpose GPU-based processing (GPGPU). In particular, memory bandwidth, instructions per second, increased programmability and higher precision arithmetic processing highlight the potential benefits. For many data-parallel computations, graphics processors outperform CPUs by more than one order of magnitude because of their streaming architecture and dedicated high-speed memory.

The introduction of CUDA [KH10] a few years ago stimulated a tremendous growth in GPU-accelerated applications. However, CUDA is a proprietary API with a set of language extensions that works only on NVIDIA's GPUs. OpenCL [TNIA10], on the other hand, is an open standard for parallel programming, maintained by the Khronos Group [Khr], which has been designed for GPGPU. OpenCL promises a portable language for GPU programming, capable of targeting very dissimilar parallel processing devices, GPU hardware, OS software, and multi-core processors.

In the next section, the mathematical formulation of the proposed algorithm and its implementation with OpenCL are described.

3. Automatic bone erosion scoring

3.1. Construction of the Statistical Shape Model

Constructing a SSM basically consists of extracting the mean shape and a number of modes of variation from a collection of training samples. Obviously, the employed methods strongly depend on the chosen shape representation.

Shape is invariant to similarity transformations (i.e., translation, rotation, and scaling). In general, shape changes induced by these global transformations should not be modeled by an SSM, in order to keep the model as specific as possible. Thus, the first step is to align all training samples in a common coordinate frame. There have been a number of works dealing with the alignment of images [CTT*01, FJ99, MMV00, VJP97, VW97]. For our application, we are interested in aligning binary images to encode the training shapes. This greatly simplifies the alignment task.

Let the training set T consist of n binary images $\{I^1, I^2, \dots, I^n\}$, each with values of one inside and zero outside the object. The goal is to calculate the set of pose parameters $\{p^1, p^2, \dots, p^n\}$ used to jointly align the n binary images, and, hence, to remove any variation in shape due to pose differences. First, a common reference image is chosen from the cohort. Based on this selection, rigid-based image registration is performed between the reference image and the remaining datasets.

The original images for the training set consists of 40 MRI volumes acquired using an Esaote C-Scan, a dedicated scanner for imaging of extremities. The sequence was a sagittal Turbo 3D T1 and the resolution was 0.55 mm x 0.55 mm in each slice with a slice thickness between 0.60 mm and

0.80 mm (with no gap slices). Each slice is 256x256 pixels and a scan has around 105 slices (Figure 2). All images are manually segmented by an expert.

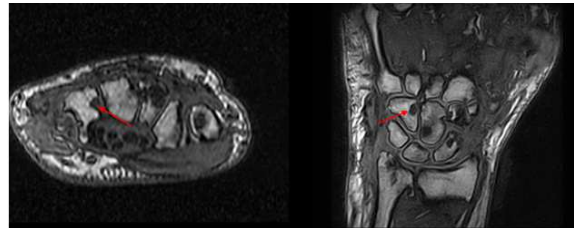


Figure 2: MRI of wrist affected by RA. The red arrow in the axial (left) and coronal (right) views highlights the same erosion of the hamate.

As mentioned earlier, a popular and natural approach to represent shapes is via point models, where a set of marker points is used to describe the boundaries of the shape. This approach suffers from problems such as numerical instability, inability to accurately capture high curvature locations, difficulty in handling topological changes, and the need for point correspondences. To overcome these problems, we utilize an Eulerian approach for shape representation based on the level-set method proposed by Osher and Sethian [OS88].

Following the lead of [OS88], we choose the signed distance function as our representation for the shape. Hence, each registered data set \tilde{I} is transferred into structure specific signed distance maps $D_a^{(i)}$, where a represents the structure of interest (Figure 3). In these distance maps, negative values are assigned to voxels within the boundary of the object, while positive values indicate voxels outside the object.

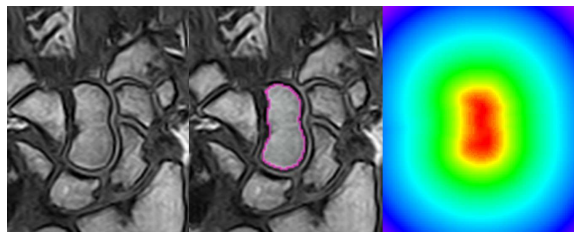


Figure 3: Distance map of the registered capitate. Coronal slice of the original MRI volume (left), segmentation of the capitate overlaid on the grayscale image (center), and registered distance map (right).

By taking the average over all these distance maps $D_a^{(i)}$, we define the mean distance map

$$\overline{D}_a = \frac{1}{n} \sum_i^n D_a^i \quad (1)$$

and the mean corrected signed distance maps

$$\tilde{D}_a^i = D_a^{(i)} - \overline{D}_a. \quad (2)$$

These mean-offset functions are then used to capture the variabilities of the training shapes through Principal Component Analysis (PCA). PCA allows to reduce the dimensionality of the training set, i.e. to find a small set of modes that best describes the observed variation. An eigen-decomposition of the related covariance matrix

$$S = \frac{1}{n-1} \sum_i^n (D_a^i - \bar{D}_a) (D_a^i - \bar{D}_a)^T \quad (3)$$

delivers the max principal modes of variation ϕ_m (eigenvectors) and their respective variances λ_m (eigenvalues).

Then, it is possible to approximate every valid shape by a linear combination of the first c modes

$$D = \bar{D} + \sum_{m=1}^c b_m \phi_m \quad (4)$$

where b_m are the weights associated to the eigenvectors ϕ_m . In many cases, c is chosen so that the accumulated variance $\sum_{m=1}^c \lambda_m$ reaches a certain ratio r of the total variance $\sum_{m=1}^{s-1} \lambda_m$. Common values for r are 0.9–0.98 (Figure 4).

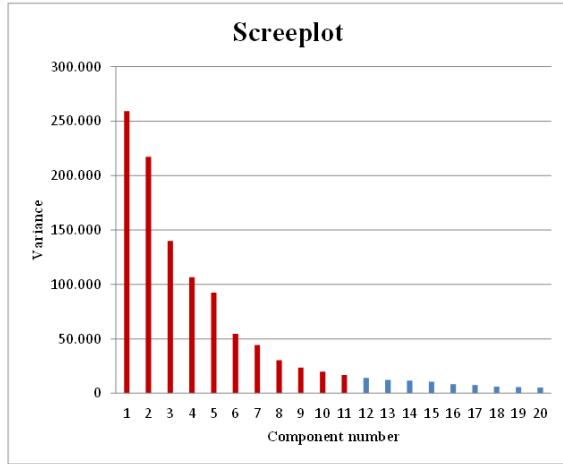


Figure 4: PCA: screeplot for the scaphoid bone. The red columns, corresponding to the first 11 components, are retained because the ratio r of the total variance is 0.9. The remaining components are discarded.

3.2. Bone reconstruction

The healthy bone of interest is reconstructed starting from its eroded shape and from the PCA describing the variability within the training set of corresponding bone healthy shapes. The reconstruction is performed in two steps, as follows:

1. *First adjustment of the real bone and the model.* In this step, the registration between the mean binary shape of the PCA and the eroded bone is performed using a rigid transformation (rotation + translation). The resulting parameters of the transformation matrix are used in the following step.

2. *Reconstruction by successive optimizations.* An evaluation function, which represents the error between the transformed model (obtained using the parameters computed in the previous step) and the real bone, is calculated. By repeating the optimization process, this evaluation function is minimized by changing the initial model (Figure 5). Modifying the initial model consists in changing the c shape parameters defined by the PCA (i.e., changing the vector of parameters weights b defined in (4)). The evaluation function chosen for this optimization process is the Dice's coefficient [Dic45]. Also known with other names, like “similarity index” or “Sørensen index”, this coefficient is used for comparing the similarity of two samples. In the bone reconstruction algorithm, the similarity is computed between the binary image of the eroded bone and the binary image of the modified initial healthy model. The Dice's coefficient d is calculated using the following formula:

$$d = \frac{2|A \cap B|}{|A \cup B|}, \quad (5)$$

in which A represents the set of the non-zero voxels belonging to the binary image of the eroded bone, B is the set of the non-zero voxels belonging to the binary image of the modified initial model.

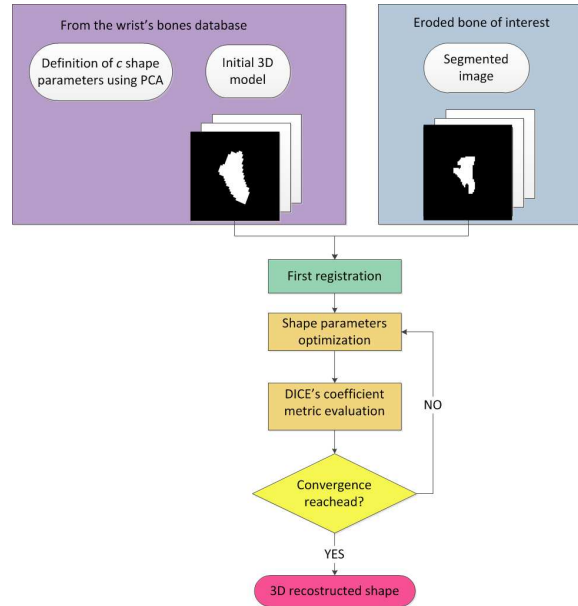


Figure 5: Overall method for the 3D reconstruction.

3.3. GPU bone reconstruction

In our implementation of the bone reconstruction algorithm on GPU, different OpenCL kernels and strategies are used to obtain a parallelism with single voxel granularity. For the

pipeline described in the previous section (Figure 5), the heavy computational effort relay in the metric evaluation.

For this reason, we write different OpenCL kernels that evaluate:

1. For the first registration step, the Kappa statistics metric [ZDMP94] between the mean binary shape of the PCA and the eroded bone. This metric is estimated for each iteration of the optimization process of the registration.
2. For each iteration of the bone reconstruction optimization process, the linear combination between the mean shape and the modes of the PCA. Moreover, another kernel evaluates the Kappa statistics metric between the resulting linear combination and the segmented eroded bone.

In order to test the speed improvement obtained using parallel computing, we implement three versions of the bone reconstruction algorithm: the first runs sequentially on the CPU, the second runs in multithread on the CPU and the last runs on the GPU via OpenCL kernels. These tests are performed on an Intel i7 processor 2.8 GHz with 6GB of RAM memory and an NVIDIA GTX260 graphic card. Tests are performed for all anatomical elements of the wrist/hand in MRI volumetric images.

As an example, in Table 1 we show the execution time of the first and second steps of our algorithm using a sequential version on CPU (CPUs), a multithread version on CPU (CPUm) and a parallel version on GPU (GPU). For the first step, the GPU version is 13 times faster than the CPUm version and 37 times faster than the CPUs. For the second step, the GPU version is 13 times faster than the CPUm version and 105 times faster than the CPUs. Similar results are obtained for the remaining bones.

Table 1: CPU versus GPU bone reconstruction for the capitate bone.

Algorithm step	Execution time (s)		
	CPUs	CPUm	GPU
First adjustment of the real bone and the model	12.37	4.43	0.33
Reconstruction by successive optimizations	114.47	18.76	1.37

In Table 2 and Table 3, we report the total execution time (CPUs, CPUm, GPU) for all the bones of the wrist district (forearm bones, carpal bones and metacarpal bones) and of the hand district (metacarpal bones and phalanx bones). As regards the wrist bones, for the first step, the GPU version results 15 times faster than the CPUm version and 42 times faster than the CPUs one. For the second step, the GPU version is 16 times faster than the CPUm one and 112 times faster than the CPUs one.

Table 2: CPU versus GPU bone reconstruction for the wrist district.

Algorithm step	Execution time (s)		
	CPUs	CPUm	GPU
First adjustment of the real bone and the model	144.26	52.35	3.4
Reconstruction by successive optimizations	2167.1	323.7	19.3

Table 3: CPU versus GPU bone reconstruction for the hand district.

Algorithm step	Execution time (s)		
	CPUs	CPUm	GPU
First adjustment of the real bone and the model	72.0	24.1	1.8
Reconstruction by successive optimizations	882.1	117.9	9.0

As regards the hand bones, for the first step, the GPU version results 12 times faster than the CPUm one and 42 times faster than the CPUs one. For the second step, the GPU version is 13 times faster than the CPUm version and 98 times faster than the CPUs one.

Moreover, in order to evaluate both the qualitative performance of the bone reconstruction algorithm and the quantitative reliability of the volume evaluation algorithm, we simulated various erosions on previously segmented healthy bones. In this way, it is possible to visually inspect the results and to understand if the algorithm could fill those manually deleted parts and reconstruct them, bringing the bone back to its original shape.

Figure 6 shows the results of the bone reconstruction algorithm when applied to healthy bones with simulated erosions. All the simulated erosions are identified by the algorithm and their shape is correctly reconstructed.

3.4. Volume and OMERACT-RAMRIS score evaluation

After reconstructing the shape of the healthy bone, the difference between the original eroded segmented bone and the reconstructed bone is computed. The resulting volume constitutes the erosion.

In order to choose the more suitable volume evaluation algorithm, some tests have been performed on phantom shapes, spheres and ellipsoids with different sizes, so as to

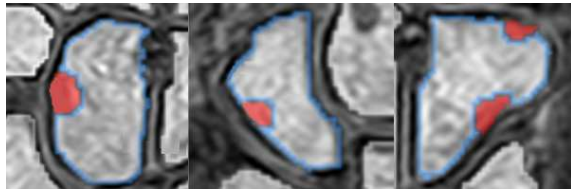


Figure 6: Bone reconstruction of simulated eroded bones. Capitulum bone (left), scaphoid bone (center), and hamate bone (right). The blue line superimposed to the MRI corresponds to the contour of the segmentation, with manually inserted holes corresponding to simulated erosions. The red part is the reconstructed part of the bone, i.e. the erosion, obtained as a result of our algorithm.

estimate the reliability of the volume evaluation algorithm (voxel counting with edge resampling - VCER) against the simple voxel counting (VC). The results show that in the case of more ideal shapes, like the spheres, the VC algorithm gives values nearest to the ideal value (VI) against the VCER algorithm. If we compute this volume on thinner, more realistic shapes (like ellipsoids), the error given by the VCER algorithm is more stable and the average value of the ratio VCER/VI is 0.98 that is nearest to the best concordance value (1) respect of the ratio VC/VI, 1.09.

In addition, we apply the VCER algorithm on healthy segmented bones and on the same bones with simulated erosions and on those reconstructed erosions (Figure 6). The error obtained comparing the “ideal” value, i.e. the VCER of the healthy segmented bone, with the “sum” of the VCER applied on the eroded bone and on the reconstructed erosions is of the same order of the previous one computed on phantom shapes.

For this reasons, we use the VCER algorithm to evaluate the volumetric information needed to compute the erosion score in accordance to RAMRIS. The global score of the erosion is computed considering the eroded bone volume compared to the intact bone, with 10% increment. As a result, the rating of the erosion per single bone is comprised between 0 (healthy bone) and 10.

4. Software application design

As the test results of our scoring procedure are very encouraging, this pipeline has been fully integrated in the RheumaSCORE application, developed by Softeco Sismat to address the RA disease [Rhe, BPV*12, CRP*13, PCVV14]. RheumaSCORE is a Computer-Aided Diagnosis (CAD) system supporting physicians (e.g. radiologist or rheumatologist) during the diagnostic process and the RA follow-up management. The physician is supported by several functional environments, addressing:

1. the *investigation*, through the recognition of wrist/hand

2. the *tracking*, through the management of clinical data (like Rheumatoid Factor and C-Reactive Protein), the insertion of free annotations and the retrieval of similar RA cases on the basis of historical clinical data, RA measurements or keywords specified in the free annotations;
3. the *follow-up*, through the automatic comparison among the parameters measured in longitudinal image pairs.

RheumaSCORE leads the user during the workflow for the evaluation of erosion scoring. The system provides a GUI where the user can select the anatomical tissue to be segmented and where the acquired images are shown. Using the Smart Brush tool [PCV*13], the user has only to “paint” some “clues” in the anatomical element to be segmented, with no need to set parameters, which are automatically adjusted by the software, or to “edit” the results. During the segmentation, the bone surface is automatically reconstructed using the marching cubes algorithm [LC87]. Once the segmentation has been completed, the system provides automatic scoring of bone erosions, using the bone reconstruction and volume evaluation algorithms, as described in the previous sections. Processing takes less than one minute for all wrist bones (or hand bones), which leads to a remarkable reduction of diagnosis time and costs.

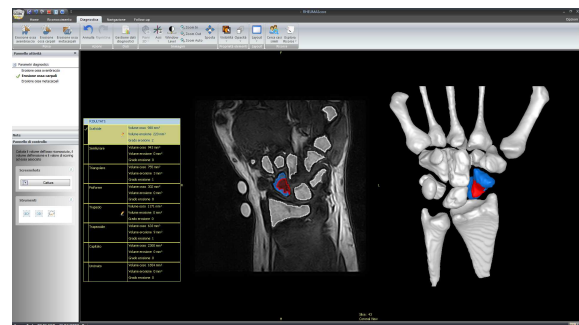


Figure 7: RheumaSCORE: diagnostic environment. The selected bone is the scaphoid. This bone is eroded and the missing part is shown in red.

Figure 7 shows the Diagnostic environment of RheumaSCORE after the bone erosion measurement. The visualization area displays

1. in the left, a table with, for each bone, the values of its volume, the volume of the erosion and the RAMRIS score. The user can change the selected bone, by clicking on the related row of the table.
2. in the middle, the simultaneous 2D slice-by-slice visualization of original grayscale data, segmentation results (in blue for the selected bone, in white for the other bones) and, only for the selected bone, its missing part reconstructed from the SSM (in red). The user can browse through the slices scrolling forward and backward and

choosing the displayed orthogonal view (axial, coronal, or sagittal). Moreover, the user can zoom and pan the image and modify the window/level and the properties displayed for the segmented/reconstructed parts.

- in the right, the 3D surface rendering of the recognized bones in blue and the missing part of the bone reconstructed from the SSM in red. The 3D scene allows the adjustment of arbitrary viewing directions and zooming into relevant regions. To support depth perception, interactive rotation is provided.

5. Clinical application

This section describes the application of our automatic scoring approach to MRI images of the wrist of patients affected by RA. We want to show the main benefits brought to the clinical practice by this novel method. The assessment in this section includes the comparison between a manual scoring by trained radiologists and the results obtained by our automatic approach. Moreover, an inter/intra operator preliminary study is presented.

5.1. RAMRIS vs RheumaSCORE

An extended and quantitative validation study has been carried out at DIMI (Dipartimento di Medicina Interna, Clinica Reumatologica, Università degli Studi di Genova). 57 patients (42 women, median age 52 years, range 20-73 years, median disease duration 22 months, range 1-420 months) diagnosed with early RA according to the 1987 ACR criteria were studied. Wrist and metacarpophalangeal (MCP) joints were imaged with a dedicated-extremity, 0.2 T MRI (Artoscan, Esaote, Genova, Italy) at baseline and after a median of 15 months (range 6-121 months).

The study was concerned on changes in RAMRIS score (single bone and total score). We found that, comparing traditional and automatic RAMRIS erosions score, perfect concordance was 45.2% at baseline and 92.9% at follow up. The correlation between the methods is reported in Figure 8, where concordance is shown in green and discordance in red for the 25 patients in whom erosion changes were seen. The x axis reports the different bones studied. Concordance was present if the reader and RheumaSCORE gave the identical RAMRIS score to the erosion. Discordance occurred in all remaining cases.

The agreement between the traditional and automatic RAMRIS evaluations was good only for the follow up MRI, after patient treatment (Figure 8). This discrepancy is apparently difficult to justify because the observers and the techniques were identical at both time points. A possible explanation is the concomitant decrease of bone marrow edema that could have occurred after successful treatment. The experienced reader is in most cases able to differentiate bone marrow edema from real erosions, whereas the automated method may be not. As a consequence, a human supervision

to correct possible imprecision of the automated procedure is still necessary.

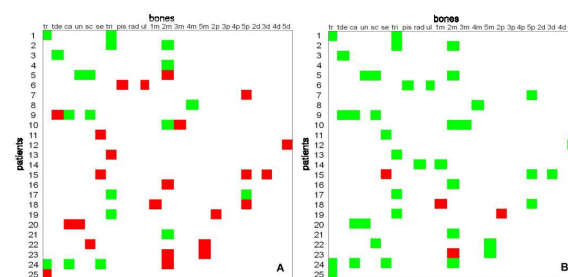


Figure 8: Correlations between traditional and semi-automated RAMRIS erosion score at baseline (A, 45.2% concordance) and at follow up (B, 92.9% concordance). Agreement is shown in green, disagreement in red.

5.2. Inter/Intra operator study

Studies for intra and inter-reader operators evaluation and for comparing the standard RAMRIS and the RheumaSCORE methods were performed: seven patients affected by RA according to the 1987 ACR criteria were studied with two MRIs with a 0.2 T dedicated machine (Artoscan, ESAOTE, Genova, Italy) using a turbo T1-weighted three dimensional sequence (T3-D T1) in the coronal plane, with subsequent multiplanar reconstructions on other planes, of the hand and wrist (baseline and follow-up 17 months apart, range 8-36 months).

The RAMRIS for erosions was calculated in agreement by two experienced readers (FB, MAC). An experienced reader (FB) and 6 inexperienced readers evaluated the 3D reconstructions of MRIs using RheumaSCORE software.

In the evaluation of bone volumes, the intra-class correlation ICC for FB in 8 consecutive readings, 2 weeks apart, was 0.99. The ICC for the inexperienced readers was again 0.99, independently from the RAMRIS for erosions. The inter-rater agreement (k) between FB and the inexperienced readers varied between 0.77 and 0.86 (mean 0.81) for patients with a low erosion RAMRIS (of value 3), and between 0.49 and 0.77 (mean 0.65) for patients with higher erosion RAMRIS (of value 9). During follow up, the median RAMRIS score for erosions remained unchanged ($p=0.12$); accordingly, also bone and erosion volumes measured by RheumaSCORE did not change ($p=0.19$).

6. Conclusion

In this work, a novel approach for automatic OMERACT-RAMRIS erosion scoring has been presented. The algorithm has been implemented exploiting the GPU parallel computation, using OpenCL. A comparison with its sequential/multithread CPU counterparts demonstrates the high

computational performance achieved. An assessment study has been carried out and preliminary results demonstrate that the use of the proposed algorithm within a dedicated software is feasible and may further facilitate the procedure of erosion staging.

Correlation values between the traditional RAMRIS and RheumaSCORE at baseline are not completely satisfactory, due to the difficulty to automatically differentiate bone marrow edema from erosions. Considering this aspect, the algorithm could be improved, e.g. considering also the information related to the image gray levels.

Moreover, the proposed method is sensitive to large bone erosions (for RAMRIS score values over 7). In this case, the large missing part in the segmented element does not allow the correct execution of the first step of the algorithm. To overcome this limitation, we plan to allow the user to correctly place the mean shape on the eroded bone, when necessary.

References

- [AAF*10] M.S. ASLAN, A. ALI, A.A. FARAG, B. ARNOLD, D. CHEN, AND P. XIANG: 3D vertebrae segmentation in CT images with random noises. *proceedings of the 2010 20th International Conference on Pattern Recognition, IEEE Computer Society*, (2010), p. 2290–3. 2
- [BEM*03] P. BIRD, B. EJBBERG, F. MCQUEEN, M. ØSTERGAARD, M. LASSERE AND J. EDMONDS: OMERACT Rheumatoid Arthritis Magnetic Resonance Imaging Studies. Exercise 5: an international multicenter reliability study using computerized MRI erosion volume measurements. *J Rheumatol*, (2003), vol. 30, pp.1380–1384. 2
- [BLSE03] P. BIRD, M. LASSERE, R. SHNIER, AND J. EDMONDS: Computerized measurement of magnetic resonance imaging erosion volumes in patients with rheumatoid arthritis: a comparison with existing magnetic resonance imaging scoring systems and standard clinical outcome measures. *Arthritis Rheum*, (2003), vol. 48, pp. 614–624. 2
- [BOG04] D. BARTZ, J. ORMAN, AND O. GURVIT: Accurate volumetric measurements of anatomical cavities. *Methods of Information in Medicine*. (2004), vol. 43, n. 4, pp. 331–335. 3
- [BPV*12] F. BARBIERI, P. PARASCANDOLO, L. VOSILLA, L. CESARIO, G. VIANO, AND M. A. CIMMINO: Assessing MRI erosions in the rheumatoid wrist: a comparison between RAMRIS and a semiautomated segmentation software. *Ann Rheum Dis*, (2012), 71 Suppl 3. 2, 7
- [CDM*11] A.R. CROWLEY, J. DONG, A. MCHAFFIE, A.W. CLARKE, Q. REEVES, M. WILLIAMS, E. ROBINSON, N. DALBETH, AND F.M. MCQUEEN: Measuring bone erosion and edema in rheumatoid arthritis: a comparison of manual segmentation and RAMRIS methods. *J Magn Reson Imaging*, (2011), vol. 33, pp. 364–371. 2
- [CLO*03] P. CONAGHAN, M. LASSERE, M. ØSTERGAARD, C. PETERFY, F. MCQUEEN, P. O’CONNOR, P. BIRD, B. EJBBERG, M. KLARLUND, R. SHNIER, H. GENANT, P. EMERY, AND J. EDMONDS: OMERACT Rheumatoid Arthritis Magnetic Resonance Imaging Studies. Exercise 4: an international multicenter longitudinal study using the RA-MRI score. *J Rheumatol*, (2003), vol. 30, pp.1376–1379. 2
- [COM*03] P. CONAGHAN, P. O’CONNOR, D. MCGONAGLE, P. ASTIN, R.J. WAKEFIELD, W.W. GIBBON, M. QUINN, Z. KARIM, M.J. GREEN, S. PROUDMAN, J. ISAACS, AND P. EMERY: Elucidation of the relationship between synovitis and bone damage: a randomized magnetic resonance imaging study of individual joints in patients with early rheumatoid arthritis. *Arthritis Rheum*, (2003), vol. 48, pp. 64–71. 2
- [CRP*13] C. E. CATALANO, F. ROBBIANO, P. PARASCANDOLO, L. CESARIO, L. VOSILLA, F. BARBIERI, M. SPAGNUOLO, G. VIANO, AND M. A. CIMMINO: Exploiting 3D part-based analysis, description and indexing to support medical applications. *Lecture Notes in Computer Science*, (2013), vol. 7723, pp. 21–32. 2, 7
- [CTG95] T.F. COOTES, C.J. TAYLOR, AND J. GRAHAM: Active shape models – their training and applications. *Comput Vis Image Underst*, (1995), vol. 61, pp.38–59. 2, 3
- [CTT*01] Y. CHEN, S. THIRUENKADAM, H. TAGARE, F. HUANG, D. WILSON, AND E. GEISER: On the incorporation of shape priors into geometric active contours. *Proc. IEEE Workshop Variational and Level Set Methods*, (2001), pp. 145–152. 4
- [Dic45] L. R. DICE: Measures of the Amount of Ecologic Association Between Species. *Ecology*, (1945), vol. 26, no. 3, pp. 297–302. 5
- [DEH*08] U. DOHN, B.J. EJBBERG, M. HASSELQUIST, E. NARVESTAD, J. MOLLER, H.S. THOMSEN, AND M. ØSTERGAARD: Detection of bone erosions in rheumatoid arthritis wrist joints with magnetic resonance imaging, computed tomography and radiography. *Arthritis Res Ther*, (2008), vol. 10, R25. 2
- [DMA*08] J. DURYEA, M. MAGALNICK, S. ALLI, L. YAO, M. WILSON, AND R. GOLDBACH-MANSK: Semiautomated three-dimensional segmentation software to quantify carpal bone volume changes on wrist CT scans for arthritis assessment. *Medical physics*, (2008), vol. 35, no. 6, pp. 2321–2330. 2, 3
- [EIC*12] P.D. EMOND, D. INGLIS, A. CHOI, J. TRICTA, J.D. ADACHI, AND C.L. GORDON: Volume measurement of bone erosions in magnetic resonance images of patients with rheumatoid arthritis. *Magn Reson Med*, (2012), vol.67, pp. 814–823. 2
- [FGC07] J.M. FARRANT, AJ GRAINGER, AND PJ O’CONNOR PJ: Advanced imaging in rheumatoid arthritis: part 2: erosions. *Skeletal Radiol*, (2007), vol. 36, pp. 381–389. 1
- [FJ99] B. FREY AND N. JOJIC: Estimating mixture models of images and inferring spatial transformations using the EM algorithm. *Proc. IEEE Conf. Computer Vision and Pattern Recognition*, (1999), vol. 1, pp. 416–422. 4
- [HM09] T. HEIMANN AND H.P. MEINZER: Statistical shape models for 3d medical image segmentation: A review. *Medical Image Analysis*, (2009), vol. 13, no. 4, pp. 543–563. 2
- [Khr] KHROS GROUP: OpenCL. <http://www.khronos.org/opencv/> 4
- [KFC89] D.N. KENNEDY, P.A. FILEPEK, AND V.S. CAVINESS: Anatomic segmentation and volumetric calculations in nuclear magnetic resonance imaging. *IEEE Trans.Med.Imag*, (1989), vol. 8, pp. 1-7. 3
- [KH10] D. KIRK AND W. HWU: Programming Massively Parallel Processors: A Hands-on Approach. *Morgan Kaufmann Publishers*, (2010). 4
- [KLZH09] D. KAINMUELLER, H. LAMECKER, S. ZACHOW, AND H.C. HEGE: An articulated statistical shape model for accurate hip Joint Segmentation. *Engineering in Medicine and Biology Society, 2009. EMBC 2009. Annual International Conference of the IEEE*, (2009), pp. 6345–6351. 3

- [KSCP11] KOCH M, SCHWING AG, COMANICIU D, AND POLLEFEYS M: Fully automatic segmentation of wrist bones for arthritis patients. In: *Proceedings of the 8th IEEE international symposium on biomedical imaging, from nano to macro, ISBI*, (2011), pp 636–640. 3
- [LC87] W. E. LORENSEN, AND H. E. CLINE: Marching Cubes: a high resolution 3D surface construction algorithm. in *proc. of ACM SIGGRAPH*, (1987), pp. 163–169. 3, 7
- [LKH*09] W LI, J KORNAK, T HARRIS, Y LU, X CHENG, AND T LANG: Hip fracture risk estimation based on principal component analysis of QCT atlas: a preliminary study. *SPIE Med Imaging*, (2009), pp. 72621M. 2
- [LMO*03] M. LASSERE, F. MCQUEEN, M. ØSTERGAARD, P. CONAGHAN, R. SHNIER, C. PETERFY, M. KLARLUND, P. BIRD, P. O'CONNOR, N. STEWART, P. EMERY, H. GENANT, AND J. EDMONDS: OMERACT Rheumatoid Arthritis Magnetic Resonance Imaging Studies. Exercise 3: an international multi-center reliability study using the RA-MRI score. *J Rheumatol*, (2003), vol. 30, pp. 1366–1375. 2
- [LVHp*06] H.M. LINDEGAARD, J. VALLØ, K. HØRSLEV-PETERSEN, P. JUNKER, AND M. ØSTERGAARD: Low-cost, low-field dedicated extremity magnetic resonance imaging in early rheumatoid arthritis: a 1-year follow-up study. *Ann Rheum Dis*, (2006), vol. 65, pp. 1208–1212. 2
- [MMV00] E. MILLER, N. MATSAKIS, AND P. VIOLA: Learning from one example through shared densities on transforms. *Proc. IEEE Conf. Computer Vision and Pattern Recognition*, (2000), vol. 1, pp. 464–471. 4
- [MSC*98] F.M. MCQUEEN, N. STEWART, J. CRABBE, E. ROBINSON, S. YEOMAN, P.L. TAN, AND L. MCLEAN: Magnetic resonance imaging of the wrist in early rheumatoid arthritis reveals a high prevalence of erosions at four months after symptom onset. *Ann Rheum Dis*, (1998), vol. 57, pp. 350–356. 2
- [OKL*01] M. ØSTERGAARD, M. KLARLUND, M. LASSERE, P. CONAGHAN, C. PETERFY, F. MCQUEEN, P. O'CONNOR, R. SHNIER, N. STEWART, D. MCGONAGLE, P. EMERY, H. GENANT, AND J. EDMONDS: Interreader agreement in the assessment of magnetic resonance images of rheumatoid arthritis wrist and finger joints – an international multicenter study. *J Rheumatol*, (2001), vol. 28, pp.1143–1150. 2
- [OPC*03] M. ØSTERGAARD, C. PETERFY, P. CONAGHAN, F. MCQUEEN, P. BIRD, B. EJBJERG, R. SHNIER, P. O'CONNOR, M. KLARLUND, P. EMERY, H. GENANT, M. LASSER, AND J. EDMONDS: OMERACT Rheumatoid Arthritis Magnetic Resonance Imaging Studies. Core set of MRI acquisitions, joint pathology definitions, and the OMERACT RA-MRI scoring system. *J Rheumatol*, (2003), vol. 30, pp. 1385–1386. 2
- [OS88] S. OSHER AND J. SETHIAN: Fronts propagation with curvature dependent speed: Algorithms based on Hamilton-Jacobi formulations. *J. Comput. Phys*, (1988), vol. 79, pp. 12–49. 4
- [PCV*13] P. PARASCANDOLO, L. CESARIO, L. VOSILLA, M. PITIKAKIS, AND G. VIANO: Smart Brush: A real time segmentation tool for 3D medical images. *Presented at Image and Signal Processing and Analysis (ISPA), 8th International Symposium on*, (2013), pp.689–694. 3, 7
- [PCVV14] P. PARASCANDOLO, L. CESARIO, L. VOSILLA, AND G. VIANO: Computer Aided Diagnosis: State-of-the-Art and Application to Musculoskeletal Diseases. *3D Multiscale Physiological Human*, Springer London, (2014) pp. 277–296. 2, 7
- [Rhe] RHEUMAScore: <http://www.research.softeco.it/rheumascore.aspx>. 2, 7
- [RCA03] M.G. ROBERTS, T.F. COOTES, AND J.E. ADAMS: Linking sequences of active appearance sub-models via constraints: an application in automated vertebral morphometry. *Presented at British Machine Vision Conference*, (2003), pp. 1–10. 2
- [Sok08] T. SOKKA: Radiographic scoring in rheumatoid arthritis: a short introduction to the methods. *Bull NYU Hosp Jt Dis*, (2008), vol. 66, pp. 166–168. 2
- [SRE*06] O. SADOWSKY, K. RAMAMURTHI, L.M. ELLINGSEN, G.I. CHINTALAPANI, J.L. PRINCE, AND R.H. TAYLOR: Atlas-assisted tomography: registration of a deformable atlas to compensate for limited-angle cone-beam trajectory. *Biomedical Imaging: Nano to Macro, 2006. 3rd IEEE International Symposium on*, (2006), pp. 1244–7. 2
- [SRS13] G. SCHETT, K. REDLICH AND, J.S. SMOLEN: Inflammation-induced bone loss in the rheumatic diseases. *Primer on the Metabolic Bone Diseases and Disorders of Mineral Metabolism*, 2nd ed., USA: John Wiley & Sons, 2013, pp. 482–488. 1
- [STCK03] SEBASTIAN TB, TEK H, CRISCO JJ, AND KIMIA BB: Segmentation of carpal bones from CT images using skeletally coupled deformable models. *Medical Image Analysis*, (2003), vpol. 7, n. 1, pp. 21-45. 3
- [TC11] Y.K. TAN AND P.G. CONAGHAN: Imaging in rheumatoid arthritis. *Best Pract Res Clin Rheumatol*, (2011), vol. 25, no. 4, pp. 569–84. 1
- [TNIA10] R. TSUCHIYAMA, T. NAKAMURA, T. IIZUKA, AND A. ASAHARA: The OpenCL Programming Book. *Fixstars Corporation*, (2010). 4
- [VJP97] T. VETTER, M. JONES, AND T. POGGIO: A bootstrapping algorithm for learning linear models of object classes *IEEE Conf. Computer Vision and Pattern Recognition*, (1997), vol. 1, pp. 40–46. 4
- [VW97] P. VIOLA AND W. WELLS: Mutual information: An approach for the registration of object models and images. *Int. J. Comput. Vis*, (1997). 4
- [WCT*15] WODARCZYK J, CZAPLICKA K, TABOR Z, WOJCIECHOWSKI W, URBANIK A: Segmentation of bones in magnetic resonance images of the wrist. *International Journal of Computer Assisted Radiology and Surgery*, (2015), vol. 10, n. 4, pp. 419-431. 3
- [WHD*11] T. WHITMARSH, L. HUMBERT, M. DE CRAENE, L.M. DEL RIO BARQUERO, AND A.F. FRANGI: Reconstructing the 3D shape and bone mineral density distribution of the proximal femur from dual-energy X-ray absorptiometry. *Med Imaging*, (2011), vol. 30, pp. 2101–2114. 2
- [ZDMP94] A. P. ZIJDENBOS, B. M. DAWANT, R. A. MARGOLIN, AND A. C. PALMER: Morphometric Analysis of White Matter Lesions in MR Images: Method and Validation. *IEEE Trans. Med. Imaging*, (1994), vol. 13, pp. 716–724. 6